Deterministic hydrodynamics: Taking blood apart

John A. Davis, David W. Inglis, Keith J. Morton, David A. Lawrence, Lotien R. Huang, Stephen Y. Chou, James C. Sturm, and Robert H. Austin

PNAS 2006;103;14779-14784; originally published online Sep 25, 2006;
doi:10.1073/pnas.0605967103

Deterministic hydrodynamics: Taking blood apart

John A. Davis*†, David W. Inglis*†, Keith J. Morton*†, David A. Lawrence‡, Lotien R. Huang*†§, Stephen Y. Chou*†, James C. Sturm*†, and Robert H. Austin*¶‖

*Princeton Institute for the Science and Technology of Materials, and Departments of †Electrical Engineering and ¶Physics, Princeton University, Princeton, NJ 08544; and ‡Wadsworth Center, Albany, NY 12201

Contributed by Robert H. Austin, July 14, 2006

We show the fractionation of whole blood components and isolation of blood plasma with no dilution by using a continuous-flow deterministic array that separates blood components by their hydrodynamic size, independent of their mass. We use the technology we developed of deterministic arrays which separate white blood cells, red blood cells, and platelets from blood plasma at flow velocities of 1,000 μm/sec and volume rates up to 1 μl/min. We verified by flow cytometry that an array using focused injection removed 100% of the lymphocytes and monocytes from the main red blood cell and platelet stream. Using a second design, we demonstrated the separation of blood plasma from the blood cells (white, red, and platelets) with virtually no dilution of the plasma and no cellular contamination of the plasma.

cells | plasma | separation | microfabrication

Human blood is a highly complex fluid containing objects of many different sizes and shapes. Blood plasma is the cell-free, clear, straw-colored fluid, which is free of objects bigger than 0.5 μm. The cell component consists of three main classes: (*i*) leukocytes or white blood cells (WBCs) are parts of the immune system, are roughly spherical, and range from 5 to 20 μm in diameter; (*ii*) erythrocytes or red blood cells (RBCs), carry oxygen to the tissue and are biconcave and discoidal (8 μm in diameter $\times$ 2 μm thick); and (*iii*) platelets range from 1 to 3 μm in diameter and are responsible for the clotting reaction (1, 2).

Traditionally, the components of blood may be fractionated according to various physical properties, including buoyant density (3) and electric charge (4), and by specific immunologic methods (5). In some of these approaches, fluorescent or magnetic particles are selectively attached to components in blood through an immunologic target. Magnetic cell sorting (MACS) and flow cytometry (FACS) are widely used methods. However, they typically require additional labels. Size, without labels, has also been used to isolate rare blood components by using filter-based methods (6). The removed component may be harvested by periodically stopping the flow into the filter and flushing to remove the desired particles from the filter mesh. Additional microfluidic methods have also included magnetophoretic separation (7) and separation by leukocyte margination (8). Size-based filter methods have also been integrated with PCR amplification of genomic DNA from WBCs (9). In general, these processes are complex, involve fluorescent labeling, yield incomplete fractionation, clog easily, or introduce bias to the data.

Previous work has demonstrated the basic separation principle of deterministic lateral displacement, a process which we also refer to as "bumping" (10). In this paper, we first review the basic deterministic lateral displacement technology, and we discuss some basic physical characteristics of the devices we have constructed, including the unusual mechanism of separation quality improving with flow rate. We then discuss the main design principles and how they affect the device operation. This discussion is extended to two different design paradigms: fractionating and preparative. The first design example is an analytical mode device designed for dispersing particles of different sizes, which we call the fractionating device (FD). The FD is demonstrated in a device to take blood apart, i.e., to individually separate RBCs and WBCs from whole blood. The results go beyond other work with WBCs (11, 12) and quantitatively analyze the output fluid by flow cytometry. The second design example is for high-throughput, and it is a preparative device called the plasma separation device (PD). It is demonstrated with the removal of all cells from whole blood to leave residual plasma.

Device Principles

In previous work, the bump array concept was introduced. A microfluidic device was used to separate 0.6- to 1.0-μm polystyrene particles with 10-nm size resolution (10). The fluid flows through an array of microposts, in which each row of posts is slightly offset laterally with respect to the previous row above it (Fig. 1). The basic principle is simple but subtle: particles below a critical hydrodynamic diameter D_c follow streamlines cyclically through the gaps, moving in an average downward flow direction. Particles above the critical hydrodynamic diameter do not fit into the first streamline and are moved by hydrodynamic lateral drag (bumped) into the sequential streamline at each post. Thus they move not parallel to the fluid flow but at an angle determined by the ratio of post offset to row–row spacing. The critical diameter D_c is just twice the width of the first streamline adjacent to the post in the gap (labeled 1 of Fig. 1), so that the center of particles above this size is bumped into the second stream line (10).

If the spacing (center to center) between the posts is called λ and the relative shift between the adjacent post rows is called d, then the parameter ε is a measure of both the relative shift and the tangent of the angle with respect to the vertical at which bumped objects move through the array (10).

$$\varepsilon = \frac{d}{\lambda} \qquad [1]$$

In general, a smaller ε results in an array with a smaller critical size. The critical hydrodynamic diameter D_c can easily be designed to be 1/3 to 1/4 the gap G between the posts (13). Thus large objects several times above the critical size are not trapped as in a filter, and the array does not easily clog at high flow rates or large particle densities. However, in a highly heterogeneous liquid such as blood in which the particle sizes differ by more than a factor of 10, simply varying ε is not enough to fractionate all components of interest. More design variations are needed to expand the range and create a nonclogging device, a point that will be addressed with one of the design approaches in this paper.

The bump array, unlike many separation technologies, relies on a deterministic process instead of a stochastic process such as diffusion. Thus faster flow rates produce less diffusional mixing of components and the performance of the device improves with increasing speed. There are two dimensionless numbers that are important in analyzing the movement of liquids in our device: the Reynolds number R_e of the fluid flow and the Peclet number P_e of the particles transported by the fluid within the device:

Conflict of interest statement: No conflicts declared.

Abbreviations: FD, fractionating device; PD, plasma separation device; PE, phycoerythrin.

§Present address: Living MicroSystems, Inc., 8 St. Mary's Street, Boston, MA 02215.

‖To whom correspondence should be addressed. E-mail: austin@princeton.edu.

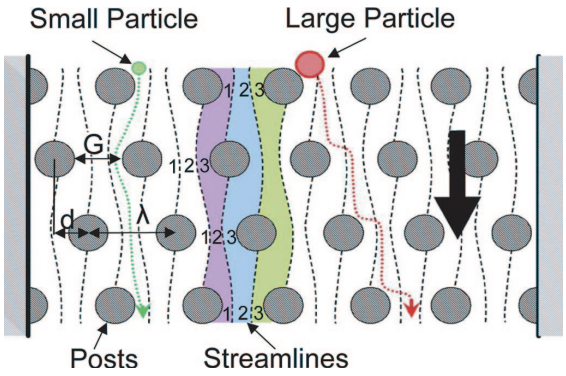

Fig. 1. Schematic illustrating the separation by deterministic lateral displacement in an array of microposts, with an example row shift fraction of one-third. This shift creates three equal flux streamlines. The dashed lines are the boundaries between the streamlines, which are assigned an index in the gaps between the posts. Paths of particles both smaller and larger than the critical threshold are depicted with green and red dotted lines respectively. Small particles stay within a flow stream and large particles are displaced at each obstacle. *G* is the clear spacing between the gap, λ is the center-to-center post separation, and *d* is the relative shift of the post centers in adjacent rows.

$$R_e \approx \frac{\rho v S}{\eta} \quad [2]$$

and

$$P_e \approx \frac{v \varepsilon L}{D}, \quad [3]$$

where ρ is the density of the fluid (in our case water at 1 g/cm^3), v is the local speed of the fluid (in our case, up to a few mm/sec), S is a characteristic length over which the fluid changes its direction (in our case, $\approx 10^{-3}$ cm), η is the viscosity of the fluid [in our case, $\approx 10^{-2}$ g/(cm·sec)], εL is a characteristic length over which diffusion competes with fluid transport (advection, about $\varepsilon\lambda$ at the local scale of the posts), and D is the diffusion coefficient of particles of radius a in the flow that we wish to separate from the flow streamlines in the bumping process. For a simple spherical object:

$$D = \frac{k_B T}{6 \pi \eta a}, \quad [4]$$

where $k_B T$ is the thermal energy at temperature T. If $R_e < 1$, the viscous damping caused by shear quickly removes kinetic energy (translational and rotational) from a fluid element and the flow is laminar with no turbulence. If $P_e > 1$ the diffusion rate is smaller than the advection rate between rows of posts and the flow is "deterministic" in that small particles are basically confined to streamlines and our bump physics works. Analysis of typical R_e and P_e numbers for ranges of size and speed within our devices is informative. The R_e is easily dealt with because we need only be assured that at the maximum flow rates $R_e < 1$. In these experiments, $v \leq 0.1$ cm/sec and $l \approx 10^{-3}$ cm, and we find that $R_e \leq 10^{-2}$, so our flow rates could go to >10 cm/sec and still be comfortably in the low R_e regime.

Unlike R_e, the P_e is not absolute for a given blood flow velocity because it is a function of particle size. Also, there are two different size scales for diffusion in our device: the local scale of the posts where diffusion moves particles out of the streamlines and ruins the deterministic bumping process, and the total array length size scale Z where diffusion broadens the lines of separated objects and ruins resolution even in the presence of successful bumping. First, we address diffusion that occurs between streamlines, while traveling the distance of a row-to-row spacing λ. If the particle diffuses into a different streamline a distance $\varepsilon\lambda$ away, its separation by bumping is compromised. In the experiments we discuss here, ε has a minimum value of 0.04 and λ has a minimum value of 5×10^{-4} cm. The smallest particles we wish to separate in this paper are blood platelets with radius $R \approx 1 \times 10^{-4}$ cm. At our typical operational speed v of 0.1 cm/sec, we find that P_e for platelets is on the order of 1×10^3, so we can safely ignore diffusion of all blood cells. Proteins (which are roughly 5 nm in radius) in the blood plasma will have a P_e of roughly 2. So whereas they will not bump because they are under the critical size, the proteins will broaden in distribution as they move through the array.

This brings up the second scale that we need to look at: the overall diffusion of small particles laterally when traveling the complete length Z of the device. This diffusion is particularly important for our analysis of proteins and ions within the plasma shown below, because diffusional broadening may result in the loss of plasma proteins into the area where the cells are bumped. This broadening can be computed simply from $x^2 = 2D(Z/v)$. The typical length of our complete device is ≈4 cm; at the typical speed of 0.1 cm/sec, a protein will diffuse a distance laterally of $\approx 10^{-2}$ cm (100 μm), whereas ions will diffuse a distance of $\approx 10^{-1}$ cm (1,000 μm). This broadening sets a limit to the purity of the "unbumped" material.

Next, we discuss very briefly a complex subject, the rotation of nonspherical objects as they move through our arrays and/or distortion of deformable shapes caused by shear. The shearing torques τ are due to the local curl $\nabla \times \vec{v}$ of the vector velocity field $\vec{v}(x, y, z)$ near surfaces, and the net force fields $\mathcal{F}$ are due to high pressure gradients ∇P as the fluid is forced through the gap G. These shearing torques and hydrostatic force fields not only can rotate and deform the cells, but in principle can lyse the cell if the shearing torques and hydrostatic pressure gradients become too high. The spatial dependence of $\vec{v}(x, y, z)$ can be computed in a straightforward way because the fluid flow is laminar, but unfortunately the calculation of the shear fields and hydrostatic forces acting on nonspherical objects is quite difficult because large objects disturb the flow fields substantially. The hydrostatic pressure gradients in our device are actually quite small even at the pressures of 1 bar (100 kPa) needed to move blood at 1,000 μm/sec through the device discussed below. We can estimate the gradient by assuming that 1/10 of the 4-cm length of the device is constricted by the gap and therefore most of the pressure drop ΔP occurs there. This means that the average pressure gradient in the gaps is roughly 2 bar/cm, which is on the order of the pressure gradients exerted on blood cells as they traverse the capillaries (14). Thus, we are not grossly out of the physiological range of hydrostatic forces, and indeed no obvious cell lysis occurs, although this observation must be checked more carefully. The rotation and distortion of compliant objects in the complex vector flow fields is a more serious issue that can change the effective critical diameter D_c. For example, an RBC has a large diameter, 8 μm, but is only 2 μm thick, so if there is a preferential orientation of the RBC in the gap flow pattern at high speeds there will be a dramatic change in bumping of the RBCs. Another possibility is that the shear fields at high flows can deform an RBC into a sausage shape (15).

Design and Methods

Array Design Principles. Our basic design principle results in a bimodal separation. A single region of posts will have a single threshold and create two directions of particle flow. Particles either travel straight through the post array or are bumped at the angle of the array. To separate a range of sizes we place a number of arrays immediately after one another, each with a slightly different critical diameter D_c. We refer to this approach as a "chirped" design. The critical diameter D_c is a function of two design parameters, which we have already discussed, the gap size G and the shift fraction ε (13). Either one of these parameters can be changed in each successive region to create the desired D_c. For example, the FD in this paper consists of 13 sections, with G fixed, and ε varied from

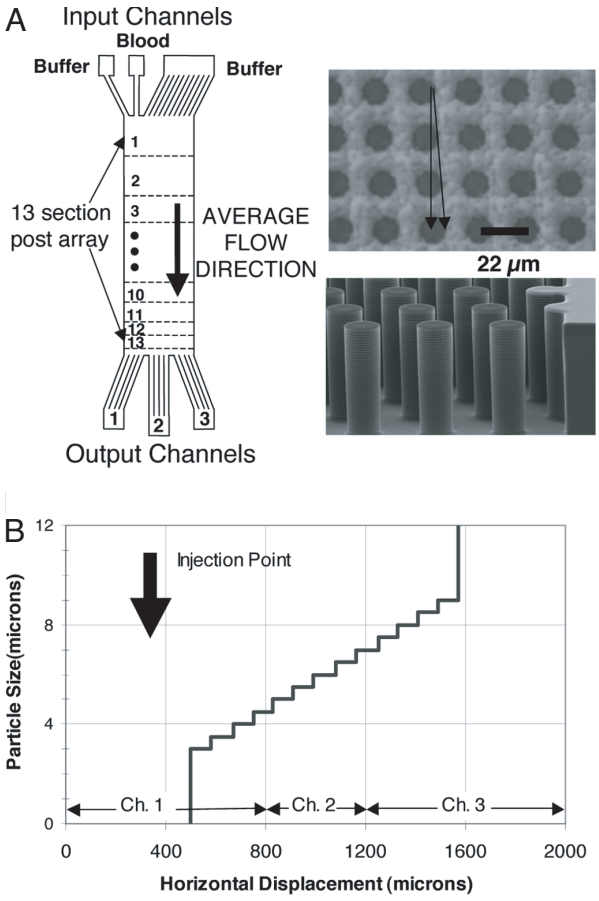

Fig. 2. The FD device designed to separate WBCs from RBCs and platelets. (*A*) (*Left*) Structure of the FD. The device consists of 13 functional regions as discussed in *Supporting Methods* (which is published as supporting information on the PNAS web site), with fixed gap G of 10 μm and varying ε. Microfluidic channels supply buffer and blood at the top and allow cells to exit at the bottom. (*Right*) (*Upper*) Microphotograph shows the top view, with the arrow indicating the vertical and bumping directions. (*Lower*) Microphotograph shows a view of posts. (*B*) The predicted input–output curve for the FD, showing particle size (hard spheres) as a function of displacement from the left wall. Also shown is the lateral position of the blood injection point at the top of the device. Three exit channels used to collect the fractionated blood and buffer samples are shown.

0.04 to 0.4. The D_c of each section varies from 3 to 9 μm at 0.5-μm intervals (Fig. 2). Particles larger than 9-μm diameter are bumped in all regions, whereas those below 3 μm flow straight through the device. Particles between 3 and 9 μm begin by bumping in the upper sections of the device, which have the smaller D_c. Once these particles enter a region in which they are below the D_c, they switch and begin flowing straight.

The dynamic range is an important evaluation of separation technologies. We define the dynamic range as the ratio of the largest to smallest critical hydrodynamic diameters that can usefully be achieved within the device. The critical diameter D_c can be made, in principle, infinitely small by choosing a small row shift fraction ε. However, this small shift results in a very low bumping angle, requiring long arrays. In practice, we find roughly $G/5$ (results from $\varepsilon = 0.02$ and bumping angle of 1°) to be a practical minimum in many situations for arrays when its fluid is driven by hydrodynamic pressure (13). In principle, the D_c can be made as large as desired by large G and ε. However, in a chirped array, the largest maximum particle size that can flow without clogging is given by the smallest gap size G. In practice, in a chirped array the dynamic range is limited to ≈3–5.

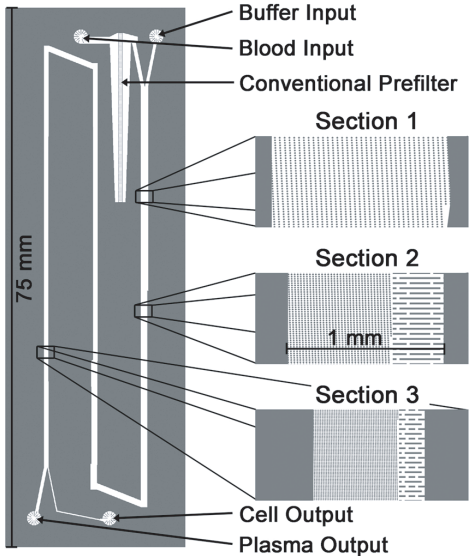

Fig. 3. The PD. Blood flows through these three successive arrays to remove cells of decreasing size. Separated blood cells bump into the serpentine pattern shown on the right of each section. See *Supporting Methods* for exact dimensions. The prefilter was designed to remove particles >20 μm.

To further increase this dynamic range, multiple (chirped or single) regions can be also be cascaded successively, each with successively smaller critical size. We will call this a "cascade" design. However, these devices need an additional feature beyond a chirped array. After the larger particles have been separated in one section, they need to be removed from the active region of the device, so as not to clog the next section. This removal can be done in a number of ways, such as exit channels at the end of each region to remove the streams with the large particles. For example, consider a cascade device consisting of two separate stages, each of which bump large particles to the right. Suppose that at the end of the first stage, the stream at the right with large particles flows to an exit port at atmospheric pressure and that the end of the second array is at atmospheric pressure as well. The pressure across the bottom of the first array (and the top of the second array) will not be uniform because of the pressure drop across the second array. This drop will cause the flow on the first and second arrays to not be precisely vertical, especially near the boundary, adversely affecting the device performance. To solve this problem, either the output ports must be held at separate pressures, or some extra fluidic resistors must be added to balance the pressure differentials of the different flow paths and restore vertical flow.

The example PD in this paper is a cascade design that shows a slightly different way to separate larger cells from successive bumping regions to prevent clogging. This device consists of three separate regions, each with a different gap: 20, 9, and 5 μm (Fig. 3). The device consists of an additional serpentine pattern on the bumping side of the device, designed to maintain straight laminar flow by matching the fluidic resistance of the array. This region collects the large particles, and prevents them from clogging the successive smaller gaps. With this or similar additions, the cascade design can have a dynamic range of 20 or more.

Table 1 summarizes the design principles of our technology. Three different types of arrays have been presented: the single array, the chirped array, and the cascade array. They each have different modes of separation, and they vary in what nonclogging dynamic range they can achieve.

We are also able to change an operational mode of the design, by changing the throat width W, the input width of the injection stream of blood. This parameter can be tailored to particular

Table 1. Design principles of bump arrays

Design principle	Mode	Nonclogging dynamic range
Single array: fixed ε, fixed G	Binary	1
Chirped array: ε or G varied	Stepped	≈3–5
Cascade array: multiple G, chirped ε	Stepped with removal of larger particles	≈20 or more

applications. A low W, on the order of the size of the gap within our device, can be used for small sample volumes and for fractionation analysis with high resolution. A high W, on the order of half of the width of the array, allows for large volumes of blood to be flowed, for example, in the removal of cells for plasma preparation.

FD. The FD is designed to separate WBCs from RBCs and plasma and fractionate the WBC according to their diameter, an analytical application. The FD has a narrow throat width (50 μm) and is designed to work with 10 μl of blood or less, not large volumes (Fig. 2). Because the main design concern is to create a high dispersion with a range in the sizes of WBCs (5–10 μm), we do not attempt to remove smaller objects such as platelets, which have a diameter on the order of 1 μm. Because the dynamic range needed is less than 4, the design can be achieved by a single chirped ε region with a constant gap G.

Fig. 2*A* shows a schematic of the FD device. Whole blood and a running buffer enter on the different channels at the top of the device, and they maintain vertical laminar flow throughout the device. The active region consists of 13 consecutive regions with a various D_c values from 3 to 9 μm (created by varying ε in a chirped design). The bumped cells are diluted into the running buffer. The FD has three separate output collection channels, each of which collects a portion of the volume of fluid exiting the device. More than three output channels would easily be possible for higher resolution; three was chosen for ease of post run analysis. The FD is designed to separate cells of slightly differing hydrodynamic radii and to put those fractionated cells into different output channels. Fig. 2*B* graphs the expected horizontal position of cells of different sizes at the end of the device according to the design criteria. Objects of progressively larger hydrodynamic radius will be displaced further and further right in each region. Cells behaving as objects larger than the maximum critical size for all 13 regions (>9 μm diameter for hard spheres) would thus be displaced ≈1,500 μm from the left edge, putting them into channel 3. Particles whose diameter is less than ≈3 μm pass straight down the device and exit in channel 1. A small number of output channels was chosen so that each one would yield a reasonable quantity of fluid that we could collect for later external analysis by conventional flow cytometry.

PD. The second example is of a preparative device, the PD. In this case, the application is the isolation of undiluted blood plasma from whole blood for further study. The device consists of a wide throat width (500 μm or one-half of the 1-mm-wide active area), so larger volumes may be prepared and high flow rates, such as 1 μl/min or more, are possible (Fig. 3). Because the device needs to remove both large (10-to 20-μm diameter) WBCs and small platelets, only the high dynamic range of a cascade device will work without clogging. In this device, the cascade consists of three different regions with three different gap sizes. Because this particular application does not require it, the individual fractionations produced in each of the regions are not maintained. Instead, all components larger than 1 μm are combined in the balanced serpentine region on the side of the device.

Fig. 3 provides a graphical picture of the layout of the PD. At the top, whole blood enters the device on the left (500 μm wide) and running buffer enters the device on the right (600 μm wide). The streams flow parallel to each and experience only diffusional mixing caused by the low Reynolds number. The cascade consists of three regions, each with a different gap. The regions each have only a single ε for this application, it would be easily possible to have each region be a chirped design if the resolution was desired. The second and third regions of the cascade have an additional balanced serpentine region, next to the active region of posts. This serpentine region has a larger minimum size, so that large particles do not clog, and we maintain our dynamic range. To maintain vertical laminar flow, the buffer portion is decreased in overall width (from 600 to 300 to 160 μm from the first section to the second and third). This causes an increase in the average vertical fluid velocity in the serpentine region, by a factor of 2 in the second region compared with the first, and 3 to 4 in the third region compared with the first.

In each region, successively smaller cells should be bumped out of the blood into the parallel stream of buffer. At the end of the device there are two outputs, one to collect the cell-free and undiluted blood plasma and one to collect the cells that have been bumped over into the buffer. At the end of all three sections, the platelets, RBCs, and WBCs are all traveling in the serpentine pattern completely bathed in buffer, while the blood plasma is still flowing on the left.

Table 2 summarizes the design of each of the two example devices presented in this paper. Both devices were constructed on 100-mm silicon wafers, patterned by standard photolithography. The features were etched by using a Bosch silicon etching process to obtain nearly vertical sidewalls. Devices were coated with a fluorosiliane vapor and sealed by glass coverslips coated with polydimethylsiloxane (PDMS) silicone on the sealing surface. Devices were placed into a Plexiglas chuck for loading and application of pressures. See *Supporting Methods* for more details.

Results and Discussion

FD. We first discuss the FD performance. Freshly drawn whole human blood (finger prick), from one of the authors, was loaded into the center running well, whereas the running buffer came from ports on the left and right sides of the specimen port (Fig. 2). Suction was applied to the exit of the device to move the blood through the device. The cells traveled at an average speed of ≈1,000 μm/sec under a negative pressure (suction) of −0.1 bar, across 1 cm of array. The throughput of analyzed blood was ≈0.3 nl/sec at this pressure gradient.

One microliter of blood was run through the FD over a period of 1 h. The fractionated components were collected at the output of each of the three exit ports. The resulting fractionated components, each of 50 μl volume, were removed from each of the exit ports with a pipette. The sample from each port was divided in half for separate analysis of RBCs and WBCs by conventional flow cytometry. To identify WBCs in the output and differentiate between different WBC subpopulations, half of each channel output was stained by using antibodies to the following: CD45 (a generic WBC marker, tagged with fluorescent Per-CP), CD19 (a B lymphocyte marker, tagged with phycoerythrin, PE), and CD3 (a

Table 2. Operation modes of prototypical bump devices

Example name	Operation mode	Injector width (W)	Design principle
Fractionation (FD)	Analytical	Narrow: on order of G	Chirped ε, fixed G
Plasma separation (PD)	Preparative	Wide: on order of half of the array width	Three cascaded regions each with different G

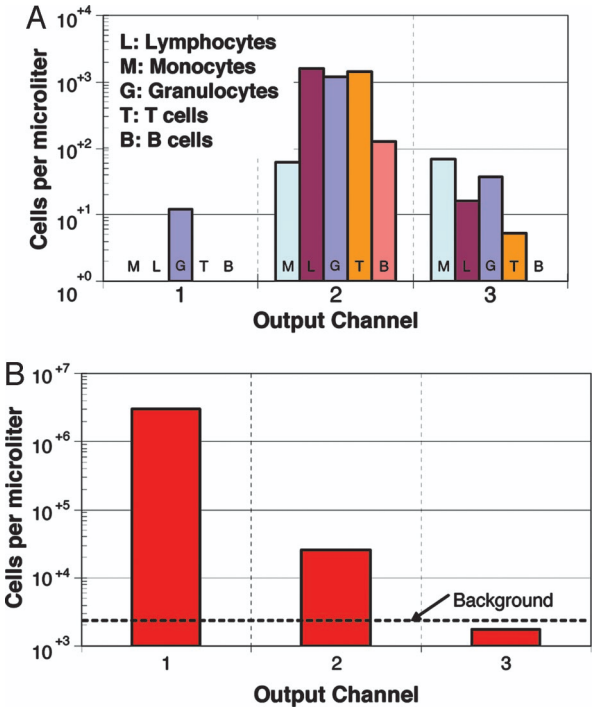

Fig. 4. WBC (*A*) and RBC (*B*) concentrations in the three output channels. WBCs analyzed were lymphocytes, monocytes, granulocytes, B cells, and T cells. Concentrations were measured with flow cytometry and Trucount beads.

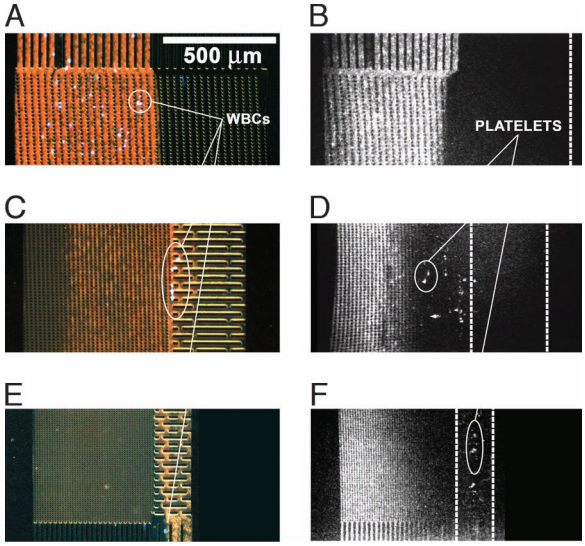

Fig. 5. Photomicrographs and brightness histograms from three places in the device. Whole blood enters the device on the left while phosphate-buffered saline enters on the right. In *B*, *D*, and *F*, the left and right borders of the serpentine region are marked with a dashed line. Flow is from top to bottom. (*A*) Whole blood with Hoechst 33342 label entering the array at the beginning of the first section. RBCs appear red and leukocytes are bluish white. (*B*) Whole blood with PE-CD41 entering the array. White areas contain higher concentrations of the fluorescent molecule. CD41 binds to platelets. (*C*) Whole blood with Hoechst 33342 label part way through the second section. Note WBCs bumped into the serpentine region entirely in the first section and RBCs have moved one third off of the right side of the bump array. (*D*) Blood with PE-CD41 part way through the second section. Some platelets are being separated from the original blood stream by the bumping process. (*E*) Whole blood with Hoechst 33342 label exiting the device. The serpentine pattern on the right carries all the cells that have been bumped out of the blood stream. (*F*) Whole blood with PE-CD41 exiting the device. The unbound fluorescent molecules remain in the blood plasma and exit the device on the left, while platelets (small white dots and streaks on the right) have been completely bumped into the serpentine region.

T lymphocyte marker, tagged with FITC). All stains were obtained from BD Biosciences (San Diego, CA). These mixtures were then lysed with FACSlyze (BD Biosciences) to remove the RBCs in the WBC population.

The second half of each mixture for the RBC analysis was not lysed. Each set of mixtures was placed into a Trucount test tube (BD Biosciences), which contains a known number of fluorescent beads, to allow calculations of cell concentrations. Both sets were analyzed on a FACScan (BD Biosciences) flow cytometer. The conventional flow cytometry analysis of forward scatter, side scatter, and three fluorescent colors was conducted. Lymphocytes, monocytes, and granulocytes were then grouped based on forward and side scatter. Lymphocyte analysis consisted of first gating on $CD45^+$ particles with low side scatter, followed by quantification of $CD19^+$ and $CD3^+$ cells by fluorescence.

Fig. 4 shows the cell counts from each of the different types of WBC and RBC. The undisplaced fluid flow from the injection channel was in channel 1. One hundred percent of the lymphocytes, monocytes, B cells, and T cells were displaced into channels 2 and 3. Cells displaced between 400 and 800 μm from the undeflected flow (800 and 1,200 μm from the wall), were ideally extracted from channel 2 (hard sphere size of 4.5–7 μm), whereas cells displaced 800–1,200 μm were ideally in channel 3 (hard sphere contact size of 7–9 μm). Conventional methods of measuring WBCs show them to be on average larger than 4.5 μm (1, 2), which agrees with our results. It is also well known that resting lymphocytes are smaller than monocytes by SEM and flow cytometry (1, 2). For lymphocytes and monocytes, the ratios of cells in channel 2 to cells in channel 3 were ≈100 to 1 and 1 to 1, respectively. The smaller lymphocytes, on average, were displaced significantly less than the larger monocytes. Most of the lymphocytes behaved like hard spheres of size smaller than 7 μm, whereas half of the monocytes were displaced below the 7-μm threshold and the other half above the threshold.

The analysis of granulocytes prevents us from claiming 100% deflection of all WBC out of channel 1. A concentration of ≈12 granulocytes per microliter per channel was calculated from flow cytometry for channel 1 (versus 1,192 and 37 for channels 2 and 3). This result limits our claim to 99% of granulocytes and 99.6% of all WBCs being displaced in channels 2 and 3. It is not known whether this granulocyte signal in channel 1 represents a real distribution of granulocytes or an ambiguous identification of granulocytes by flow cytometry. Because of the well known tendency of granulocytes to produce a wide range of forward and side scattering intensities, background counts may be incorrectly identified as granulocytes, especially because there is no definitive marker for granulocytes.

The second flow cytometric analysis was designed to measure the number of RBCs in each output channel. All cells producing forward and side scatter in the flow cytometry were counted as potential cells (except the Trucount beads) and the expected WBCs in each channel (based on the lysed blood values) were subtracted to give a raw RBC count for each channel (Fig. 4*B*). A total of 3×10^6 RBCs were detected, with 99% of the RBCs in channel 1. A flow cytometry analysis of the Trucount beads and our running buffer without blood gave a background concentration of ≈2,000 particles per microliter within the forward and side scatter area used for flow cytometry analysis of WBCs and RBCs. Thus, the concentration of RBCs in channel 3 (raw signal of 1,900 particles per microliter) is not significant and is probably due to this background. There were a statistically significant number of RBCs in channel 2 (26,000 cells per microliter or 0.9% of the total RBCs), which act as hard sphere particles of size 4.5–7 μm. It is not known whether this result is due to a second-order effect, an aberrant RBC

population, or some other nonideality. Nevertheless, an enrichment of the WBC to RBC ratio of over 110-fold from that of the initial blood specimen was obtained from channel 2 of our microfluidic device.

PD. We now discuss the performance of the PD. Fig. 5 presents photomicrographs and fluorescence intensity scans from three places in the device. Images are from the beginning of the first section, the middle of the second section and the end of the third section. Three different blood samples were run in the PD. One sample (Fig. 5 *Left*) was designed to look at the removal of RBCs and WBCs from the plasma. It was incubated with Hoechst 33342 to stain the WBC nuclei, whereas the RBCs were observed by using white light. The second sample (not shown in Fig. 5) was designed to monitor the more challenging task of the removal of platelets and was incubated with PE-conjugated CD41 antibodies to specifically label blood platelets, the smallest cells (1 μm) normally occurring in blood. The unbound PE-CD41 was washed out of the sample before running. In this experiment, no platelets were observed in the plasma stream at the end of the device. The third sample (Fig. 5 *Right*) was designed to verify the flow of the cell-free plasma. In this case, the unbound PE-CD41 was not washed before the blood was run. The fluorescence of the unbound PE-CD41 in the blood was used to image the flow of the blood plasma. As in the second sample, platelets were easily identified as bright spots, whereas unbound PE-CD41 was identified as a uniformly bright fluorescent background.

Freshly drawn whole human blood (finger prick) was used. The stained blood was loaded into the left running well, whereas the running buffer came from a port on the right side of the specimen port. A common pressure was applied to both the blood and buffer ports. At a pressure of 0.3 bar (0.5 pound per square inch) the observed volume of blood flow through the present device was $\approx$0.4 μl/min, with a flow from top to bottom in Fig. 5. The active area is on the left, whereas the serpentine region on the right carries cells that have been bumped out of the blood stream. Over the first region, nucleated cells (WBCs) and a small percentage of RBCs were observed to travel in the bump mode. Note in Fig. 5*C* all of the WBCs are in the serpentine region, with none in the second array. Most RBCs and some platelets are observed to travel in bump mode in the second section, placing these cells in the buffer stream. In Fig. 5*C* (partly through the second section), RBCs have been removed from the left third of the array. Note also in Fig. 5*D* (partly through the second section) that some platelets have been removed from the original blood stream (with the unbound dye giving a white background to show the stream). At the end of section three, the platelets, RBCs, and WBCs are all traveling in the serpentine pattern completely bathed in buffer, whereas the blood plasma is still flowing on the left.

The most important observation in Fig. 5 is the intensity of the unbound PE-CD41 dye. Because that fluorescence intensity comes from a molecular species, it tracks the movement of the protein components of plasma. As Fig. 5*F* shows, the dye remains on the left side of the chamber, and all of the plasma in the blood can be recovered essentially undiluted. The unbound fluorescent molecules remain in the blood plasma and exit the device on the left, free of platelets and cells. The width of the blood plasma stream is less than the width of the incoming blood stream, because half of the volume of the blood is composed of the cells which have been removed. The PD chip has succeeded in removing all of the blood cell objects of size >1 μm, including platelets, while maintaining the blood plasma in its undiluted state with, in principle, 100% recovery.

The observed width of the dye stream in Fig. 5*F* is not a straight vertical line at the end of the device because of an inadvertent hydrodynamic impedance mismatch between the third section and the output channels. This mismatch causes the stream to widen near the exit. Even before this broadening of the plasma stream at the end due to inadvertent mismatch, the right edge of the dye molecules in the plasma stream near the end of the device is not as sharp as at the top, however. This transition width is $\approx$100 μm, consistent with the expected lateral diffusion of the molecules as discussed near the end of *Device Principles*.

Conclusions

We have shown two different example designs of a hydrodynamic bump technology. A complex fluid such as blood can be separated in two different ways: by using a narrow focused hydrodynamic jet, the blood cells can be fractionated as a function of their diameter in an analytical manner; and by using a broad stream a preparative sample can be made with all of the particulates in blood removed, leaving behind plasma that has not been diluted in the process. Further work will involve increasing the resolving power of the fractionating device and moving the minimum size resolution down to the bacterial and possibly viral level, and increasing the flow rate in the preparative device to where microliter volumes of blood can be processed in a few minutes time.

We thank the members of our laboratories for helpful discussion and Eric Eisenstadt for his continuous encouragement and advice. We also acknowledge the Cornell University National Fabrication Center, where some of the deep silicon etching process of the device reported here was performed. This work at Princeton was supported by Defense Advanced Research Projects Agency/Office of Naval Research Grants W911NF-05-1-0392, N00014-04-1-0776, and MDA972-00-1-0031; National Science Foundation Nanobiology Technology Center Grant BSCECS9876771; and New Jersey Commission on Science and Technology Grant NJCST99-100-082-2042-007.

1. Schmid-Schonbein GW, Shih YY, Chien S (1980) *Blood* 56:866–875.
2. Dacie JV, Lewis SM (2001) *Practical Haematology* (Churchill Livingstone, London).
3. Boyum A (1974) *Tissue Antigens* 4:269–274.
4. Wachtel D, Sammons D, Manley M, Wachtel G, Twitty G, Utermohlen J, Phillips OP, Shulman LP, Taron DJ, Muller UR, *et al.* (1996) *Hum Genet* 98:162–166.
5. Smeland EB, Funderud S, Blomhoff HK, Egeland T (1992) *Leukemia* 6:845–852.
6. Mohamed H, McCurdy LD, Szarowski DH, Duva S, Turner JN, Caggana M (2004) *IEEE Trans Nanobiosci* 3:251–256.
7. Han KH, Frazier AB (2004) *J Appl Phys* 96:5797–5802.
8. Shevkoplyas SS, Tatsuro Y, Munn LL, Bitensky MW (2005) *Anal Chem* 77:933–937.
9. Panaro NJ, Lou XJ, Fortina P, Kricka LJ, Wilding, P (2005) *Biomol Eng* 21:157–162.
10. Huang LR, Cox EC, Austin RH, Sturm JC (2004) *Science* 304:987–989.
11. Zheng S, Yung R, Tai Y, Kasdan H (2005) *Proceedings of the IEEE International Conference on Micro Electro Mechanical Systems* (IEEE), Vol 17, pp 851–854.
12. Zheng S, Tai Y, Kasdan H (2005) *Proceedings of μTAS* (Transducer Research Foundation, San Diego), pp 385–387.
13. Inglis DW, Davis JA, Austin RH, Sturm JC (2006) *Lab Chip* 6:655–658.
14. Pries AR, Secomb TW, Gaehtgens P (1995) *Circ Res* 77:1017–1023.
15. Gifford SC, Frank MG, Derganc J, Gabel C, Austin RH, Yoshida T, Bitensky MW (2003) *Biophys J* 84:623–633.